

# Atomistic study of grain-boundary segregation and grain-boundary diffusion in Al-Mg alloys

R. K. Koju<sup>1</sup> and Y. Mishin<sup>1</sup>

<sup>1</sup>*Department of Physics and Astronomy, MSN 3F3,  
George Mason University, Fairfax, Virginia 22030, USA*

(Dated: October 15, 2020)

Mg grain boundary (GB) segregation and GB diffusion can impact the processing and properties of Al-Mg alloys. Yet, Mg GB diffusion in Al has not been measured experimentally or predicted by simulations. We apply atomistic computer simulations to predict the amount and the free energy of Mg GB segregation, and the impact of segregation on GB diffusion of both alloy components. At low temperatures, Mg atoms segregated to a tilt GB form clusters with highly anisotropic shapes. Mg diffuses in Al GBs slower than Al itself, and both components diffuse slowly in comparison with Al GB self-diffusion. Thus, Mg segregation significantly reduces the rate of mass transport along GBs in Al-Mg alloys. The reduced atomic mobility can be responsible for the improved stability of the microstructure at elevated temperatures.

Keywords: Atomistic modeling; Al-Mg alloys; grain boundary segregation; grain boundary diffusion.

## I. INTRODUCTION

Al-Mg alloys constitute an important class of lightweight structural materials that find numerous automotive, marine and military applications [1]. Mg improves many mechanical properties of Al, such as tensile and fatigue strength, ductility, and weldability [1–4], while maintaining a high strength to weight ratio and a relatively low production cost. Progress in designing more advanced Al-Mg alloys requires further improvements in the fundamental knowledge of the Mg effect on the microstructure and properties.

Previous experimental and modeling studies have shown that Mg segregates to Al grain boundaries (GBs), modifying their thermodynamic and kinetic properties [3–10]. Mg segregation was found to increase both the strength and ductility of Al, as well as thermal stability of the grains [3, 4, 8, 10]. The stability improvement is attributed to a combination of the thermodynamic reduction in the GB free energy and the pinning of GBs by solute atoms due to the solute drag effect. It should be emphasized that the solute drag process is controlled by diffusion of the solute atoms in the GB region [11–15]. Diffusion must be fast enough to move the segregation atmosphere along with the moving boundary. If diffusion is too slow and/or the GB motion too fast, the boundary breaks away from the

segregation atmosphere and the drag force abruptly drops [11, 14]. On the other hand, fast GB diffusion promotes coarsening of the microstructure by accelerating the mass transport of the alloy components. A detailed understanding of the GB diffusion process and its relationship with solute segregation is a prerequisite for rational design of Al-Mg alloys.

When the Al matrix is supersaturated with Mg, the excess Mg atoms diffuse toward and then along GBs and precipitate in the form of the  $\text{Al}_3\text{Mg}_2$  phase and/or possibly other, metastable compounds [4, 16, 17]. Such precipitates usually have a detrimental effect by causing, for example, corrosion cracking and other undesirable consequences [18]. The GB precipitation process depends on the level of GB segregation and the rate of Mg GB diffusion.

Surprisingly, while Al GB diffusion in Mg has been measured [19, 20], to the best of our knowledge, Mg GB diffusion coefficients in Al or Al-Mg alloys have not been measured experimentally or predicted by simulations. The only paper known to us [21] contains highly indirect estimates of the triple product  $s\delta D$  ( $s$  being a segregation parameter,  $\delta$  the GB width, and  $D$  the GB diffusion coefficient)\* based on electromigration experiments in thin films at one temperature. These measurements do not provide a complete or reliable quantitative information on Mg GB diffusion coefficients.

In this paper, we report on detailed atomistic computer simulations of GB segregation and GB diffusion in the Al-Mg system, focusing on a particular Al-5.5at.%Mg composition relevant to industrial alloys. Two representative GBs were selected, a high-angle tilt GB composed of closely spaced structural units, and a low-angle twist GB composed of discrete dislocations. The latter case essentially probes the dislocation segregation effect and the dislocation pipe diffusion. In addition to computing some of the key characteristics of Mg GB segregation over a range of temperatures, the simulations reveal some interesting features of the segregation, such as the formation of Mg clusters in the high-angle GB and the tendency of the clusters to have highly elongated shapes reminiscent of linear atomic chains. The diffusion coefficients and Arrhenius parameters have been computed for GB diffusion of both Al and Mg, and are compared with Al GB self-diffusion as well as diffusion of both components in liquid alloys.

## II. METHODOLOGY

Atomic interactions in the Al-Mg system were modeled using the Finnis-Sinclair potential developed by Mendeleev et al. [23]. The potential provides an accurate description of the Al-rich part of the phase diagram and predicts the melting temperatures of Al and Mg to be 926 K [24] and 914 K [25], respectively, in good agreement with experimental data (934 and 922

---

\* The units of  $s\delta D$  were not given in [21], but it was later suggested [22], based on previous papers of these authors, that they could be  $\text{cm}^3 \text{s}^{-1}$ .

K, respectively). The software package LAMMPS (Large-scale Atomic/Molecular Massively Parallel Simulator) [26] was utilized to conduct molecular statics, molecular dynamics (MD), and Monte Carlo (MC) simulations. Visualization and structural analysis were performed using the OVITO software [27].

The high-angle GB studied here was the symmetrical tilt  $\Sigma 17(530)[001]$  GB with the misorientation angle of  $61.93^\circ$ . The parameter  $\Sigma$  is the reciprocal density of coincident sites,  $[001]$  is the tilt axis, and  $(530)$  is the GB plane. This boundary was created by aligning the crystallographic plane  $(530)$  parallel to the  $x$ - $y$  plane of the Cartesian coordinate system and rotating the upper half of the simulation block ( $z > 0$ ) by  $180^\circ$  about the  $z$ -axis. The low-angle GB was the  $\Sigma 3601(001)$  twist boundary with the misorientation angle of  $1.91^\circ$ . In this case, the GB plane is  $(001)$  and the two lattices are rotated relative to each other about the common  $[001]$  axis. The simulation blocks had approximately square cross-sections parallel to the GB plane. The block dimensions in the  $x$ ,  $y$  and  $z$  directions were, respectively,  $11.79 \times 11.73 \times 23.67$  nm ( $1.97 \times 10^5$  atoms) for the high-angle GB and  $24.27 \times 24.27 \times 48.56$  nm ( $1.72 \times 10^6$  atoms) for the low-angle GB. Periodic boundary conditions were imposed in all three directions.

The initial GB structures were optimized by the  $\gamma$ -surface method [28–30]. In this method, one grain is translated relative to the other by small increments parallel to the GB plane. After each increment, the total energy is minimized with respect to local atomic displacements and rigid translations of the grains normal to the GB plane (but not parallel to it). The minimized GB energy is plotted as a function of the translation vector, producing a so-called  $\gamma$ -surface. The translation vector corresponding to the deepest energy minimum on the  $\gamma$ -surface is identified, and the total energy is further minimized by allowing arbitrary atomic displacements in all three directions starting from this translational state. The GB structure obtained is considered the closest approximation of the ground state of the boundary.

To create a thermodynamically equilibrium distribution of Mg atoms in the Al-5.5at.%Mg alloy, the hybrid MC/MD algorithm [31] was implemented in the semi-grand canonical NPT ensemble (fixed total number of atoms  $N$ , fixed temperature  $T$ , and zero pressure  $P$ ). Every MC step was followed by 250 MD steps with the integration time step of 2 fs. The imposed chemical potential difference between Al and Mg was adjusted to produce the desired chemical composition inside the grains. The simulation temperature varied between 350 K and 926 K.

GB diffusion was studied by NPT MD simulations in the temperature range from 400 K to 926 K using the GBs pre-equilibrated by the MC/MD procedure. During the MD runs, the GB position could slightly vary due to thermal fluctuations. To account for such variations, the instantaneous GB position was tracked by finding the peak of the potential energy (averaged over thin layers parallel to the GB plane) as a function the  $z$  coordinate normal to the boundary. The GB position was identified with the center of the peak, while

the GB width  $\delta$  was estimated from the peak width. Based on these estimates, the GB core region was defined as the layer centered at the peak and having the width of  $\delta = 1$  nm for the high-angle GB and  $\delta = 1.5$  nm for the low-angle GB. The mean-square displacements,  $\langle x^2 \rangle$  and  $\langle y^2 \rangle$ , of both Al and Mg atoms parallel to the GB plane were computed as functions of time. The calculations extended over a time period  $\Delta t$  ranging from 0.03 ns to 120 ns, depending on the temperature. The GB diffusion coefficients of both species were extracted from the Einstein relations  $D_x = \langle x^2 \rangle / 2\Delta t$  and  $D_y = \langle y^2 \rangle / 2\Delta t$ , respectively. For comparison, similar calculations were performed for Al self-diffusion in both GBs. In this case, the pure Al boundary was equilibrated by a 2 ns MD run before computing the mean-square displacements. For the low-angle GB, the symmetry dictates that  $D_x$  and  $D_y$  must be equal. Accordingly, the diffusion coefficients reported for this boundary were averaged over both directions.

For further comparison, the same methodology was applied to compute the diffusion coefficients of Al and Mg in the liquid Al-5.5at.%Mg alloy at temperatures close to the solid-liquid coexistence (solidus) line. The simulation block had the dimensions of  $11.73 \times 11.73 \times 11.73$  nm ( $\sim 10^5$  atoms) and was equilibrated by an MD run for a few ns prior to diffusion calculations.

### III. RESULTS AND ANALYSIS

#### A. Grain boundary structures and energies

The excess energy of the equilibrated high-angle  $\Sigma 17$  GB was found to be  $488 \text{ mJ m}^{-2}$ . The 0 K structure of this boundary consists of identical kite-shape structural units arranged in a zigzag array as shown in Fig. 1a. The rows of these structural units running parallel to the tilt axis (normal to the page) can be interpreted as an array of closely spaced edge dislocations forming the GB core. An identical zigzag arrangement of the kite-shape units in this GB was earlier found in Cu [15, 32–34] and Ni [35], suggesting that this atomic structure is common to FCC metals.

The low-angle  $\Sigma 3601$  GB has a smaller energy of  $127 \text{ mJ m}^{-2}$  and consists of a square network of discrete dislocations (Fig. 1b). As expected from the dislocation theory of GBs [36], the dislocation lines are parallel to the  $\langle 110 \rangle$  directions and have the Burgers vectors of  $\mathbf{b} = \frac{1}{2} \langle 110 \rangle$ . Furthermore, the Frank formula [36] predicts that the distance between parallel GB dislocations in the network must be approximately  $|\mathbf{b}|/\theta$ , where  $\theta$  is the twist angle. Examination of the GB structure reveals that this prediction is indeed followed very closely.

## B. Grain boundary segregation

Mg was found to segregate to both GBs at all temperatures studied. The images in Fig. 2 illustrate the equilibrium distributions of the Mg atoms along with the atomic disorder of the GB structures at the temperature of 700 K.

Equilibrium segregation profiles were computed by averaging the atomic fraction of Mg over thin layers parallel to the GB on either side of its current position. The composition profiles displayed in Fig. 3 were averaged over multiple snapshots during the MD/MC simulations after thermodynamic equilibration. The following features of the segregation profiles are noted:

- Mg segregates to the high-angle GB much stronger than to the low-angle GB.
- The height of the segregation peak increases with decreasing temperature, reaching about 21 at.%Mg in the high-angle GB and about 7 at.%Mg in the low-angle GB at the lowest temperature tested.
- At high temperatures approaching the melting point of the alloy ( $> 850$  K), the segregation profile of the high-angle GB significantly broadens, suggesting that the boundary undergoes a premelting transformation.

At temperatures between 860 and 870 K, the premelted high-angle GB was observed to extend across the entire simulation block, transforming it into the bulk liquid phase. Based on this observation, the solidus temperature of the alloy was estimated to be  $865 \pm 5$  K. This estimate compares well with the equilibrium phase diagram obtained by independent calculations in [23]. The low-angle GB did not premelt and could be readily overheated above the solidus temperature, keeping the dislocation network intact albeit with highly disordered dislocation cores.

The amount of segregation was quantified by computing the excess number of Mg atoms per unit GB area at a fixed total number of atoms:

$$[N_{\text{Mg}}] = N_{\text{Mg}} - N \frac{N'_{\text{Mg}}}{N'}. \quad (1)$$

Here,  $N_{\text{Mg}}$  and  $N'_{\text{Mg}}$  are the numbers of Mg atoms in two regions with and without the GB, respectively, and  $N$  and  $N'$  are the total numbers of Al and Mg atoms in the respective regions. These regions were chosen to have the same cross-sectional area parallel to the GB, and the excess  $[N_{\text{Mg}}]$  was normalized by this area. Accordingly, the units of  $[N_{\text{Mg}}]$  reported here are the number of excess Mg atoms per nanometer squared. The average value and standard deviation of  $[N_{\text{Mg}}]$  were obtained by averaging over multiple snapshots generated during the MC/MD simulations. Fig. 4 shows the amount of Mg segregation as a function of temperature. As expected from the segregation profiles (cf. Fig. 3),  $[N_{\text{Mg}}]$  decreases with

increasing temperature and is much higher for the high-angle GB than for the low-angle GB.

An alternative measure of the Mg segregation is the atomic fraction  $c_{GB}$  of Mg atoms in the GB computed by averaging over a layer of the Gaussian width centered at the concentration peak (cf. Fig. 3). The GB concentrations obtained are expected to follow the modified Langmuir-McLean segregation isotherm [37]

$$\frac{c_{GB}}{\alpha - c_{GB}} = \frac{c}{1 - c} \exp\left(-\frac{F_s}{kT}\right). \quad (2)$$

Here,  $c$  is the alloy composition (atomic fraction of Mg),  $k$  is Boltzmann's constant,  $F_s$  is the segregation free energy per atom, and  $\alpha$  is the fraction of GB sites filled by Mg atoms when the segregation is fully saturated.  $F_s$  represents the difference between the free energies of Mg atoms inside the GB and in the grain interiors. For both GBs, the temperature dependence of  $c_{GB}$  could be fitted by equation (2) reasonably well, see Fig. 5, with the values of  $F_s$  and  $\alpha$  listed in Table I. For the low-angle GB, the quality of fit is somewhat lower because  $c_{GB}$  is significantly closer to  $c$ . The negative values of  $F_s$  indicate that the interaction between the Mg atoms and the GBs is attractive. The absolute values of  $F_s$  are also meaningful and consistent with previous reports. For example, Mg segregation energies in Al  $\Sigma 5$  [001] tilt and twist GBs were found to be  $-0.50$  eV and  $-0.20$  eV, respectively [6]. A more recent first-principles study of the Al  $\Sigma 5$  [001] tilt boundary reports the Mg segregation energy of  $-0.3$  eV [38]. For the Al  $\Sigma 11$  [311] tilt GB, first-principles calculations predict the Mg segregation energies of  $-0.02$  eV,  $-0.070$  eV and  $-0.185$  eV for three different GB sites [7]. It should be noted that the calculations in [6] utilized a different interatomic potential, and that the values reported in the literature represent the segregation energy, not free energy. The free energy obtained here additionally includes the effects of the vibrational and configurational entropies. Furthermore, GB structures typically exhibit a diverse set of atomic environments, and thus a wide spectrum of segregation energies. The values of  $F_s$  reported in Table I should be interpreted as representative (effective) values. The saturation parameter  $\alpha$  is understood as the fraction of the GB sites with the largest magnitude of  $F_s$ . Given these uncertainties, we consider our results to be in reasonable agreement with the literature and consistent with the physical meaning of segregation parameters.

A peculiar segregation feature was found in the high-angle GB. While most of the Mg atoms were distributed in the GB in a random manner, a tendency to form Mg clusters was observed, especially at low temperatures. Cluster analysis was performed on statically relaxed snapshots using the OVITO software [27]. An example of clusters is shown in Fig. 6. To reveal the clustering effect more clearly, only clusters containing 10 or more atoms are visualized. Figure 7a shows the cluster size distribution at different temperatures (size being defined as the number of atoms in the cluster). Only clusters containing 6 or more atoms are included in the distribution. Since such clusters constitute a tiny fraction of the

entire cluster population in the GB, their contribution would be nearly invisible if smaller clusters were included in the distribution. At most temperatures, it was not unusual to see clusters containing 10 or more atoms. In fact, even clusters containing 30 to 40 atoms were occasionally seen at low temperatures. It should be emphasized that the clusters discussed here are not a static feature of the GB structure. Instead, they behave as dynamic objects that randomly form and dissolve during MD simulations, constantly changing their size, shape and location by exchanging Mg atoms with each other and with the bulk solution. The clustering of segregated atoms is a clear sign of attractive solute-solute interactions inside the GB core.

It should also be noted that the clusters shapes are significantly elongated along the tilt axis. This elongation was quantified by the eccentricity parameter

$$e = \sqrt{1 - \frac{1}{2} \left( \frac{l_y}{l_x} \right)^2 - \frac{1}{2} \left( \frac{l_z}{l_x} \right)^2}, \quad (3)$$

where  $l_x$  represents the cluster dimension along the tilt direction, and  $l_y$  and  $l_z$  are the respective dimensions in the two perpendicular directions. The eccentricity was calculated only when the dimension along the tilt axis was longer than in the perpendicular directions, and was assigned a zero value otherwise. As evident from Fig. 7b, the cluster elongation tends to increase (larger  $e$ ) with the cluster size and decrease with temperature. Large clusters containing 20 or more atoms looked almost like linear chains.

### C. Grain boundary diffusion

Figure 8 shows representative  $\langle x^2 \rangle$  versus time plots whose slopes were used for computing the GB diffusion coefficients. The plots are fairly linear as expected from the Einstein relation. The slopes of the plots indicate that Al GB self-diffusion is faster than Al GB diffusion in the alloy, which in turn is faster than Mg GB diffusion in the alloy. For the high-angle GB, this trend holds at all temperatures studied here. In the low-angle GB, Al and Mg diffuse at approximately the same rate, and both are slower in comparison with Al self-diffusion.

The results of the diffusion calculations are summarized in the Arrhenius diagram,  $\log D$  versus  $1/T$ , shown in Fig. 9. For the high-angle GB, the diffusion coefficients are reported separately for both directions, parallel and perpendicular to the tilt axis. Diffusion in the high-angle GB is several orders of magnitude faster than diffusion in the low-angle GB at all temperatures. This behavior is typical for metallic systems as reviewed in [39–41]. The diffusion coefficients closely follow the Arrhenius relation

$$D = D_0 \exp \left( -\frac{E}{kT} \right) \quad (4)$$

at all temperatures below the solidus temperature. Note that Mg segregation reduces or even eliminates the diffusion anisotropy in the high-angle GB. In pure Al, diffusion along the tilt axis is faster than in the direction normal to the tilt axis. This trend is general and was observed in both experiments and previous simulations, for example in Cu and Cu-Ag alloys [29, 32, 42, 43]. In the Al-Mg alloy, the anisotropy of Al GB diffusion is significantly smaller in comparison with that of self-diffusion in pure Al. Furthermore, GB diffusion of Mg is practically independent of the direction.

Table II summarizes the activation energies  $E$  and pre-exponential factors  $D_0$  obtained by fitting Eq.(4) to the simulation data. For the low-angle GB, the diffusivity follows the Arrhenius relation even above the solidus temperature, which allowed us to include one extra point (900 K) into the fit. Note that the activation energies follow the trend  $E_{\text{Al-Al}} < E_{\text{Al-Alloy}} < E_{\text{Mg-Alloy}}$ , suggesting that the observed retardation of GB diffusion by Mg segregation is primarily caused by increase in the activation energy. This is also evident from the converging behavior of the Arrhenius lines in Fig. 8, leading to very similar diffusion coefficients of Al and Mg close to the melting point.

In pure Al, the self-diffusivity in the high-angle GB was also computed at two additional temperatures (900 and 914 K) lying above the alloy solidus temperature but below the Al melting point (926 K). At these temperatures, the boundary develops a highly disordered atomic structure similar to a liquid layer. Accordingly, the GB diffusion coefficient shows a significant upward deviation from the Arrhenius behavior and approaches the self-diffusion coefficient in liquid Al (see inset in Fig. 8). A similar behavior was previously observed in the same  $\Sigma 17$  GB in Cu [32]. It is interesting to note that Al diffuses in the liquid alloy somewhat slower than in pure Al, and Mg diffused even slower. This trend mimics the similar behavior of GB diffusion, suggesting that the underlying cause is the nature of atomic interactions in the Al-Mg system rather than details of the GB structures.

#### IV. DISCUSSION

Atomistic simulations of GB structure, solute segregation and GB diffusion are computationally expensive and have only been performed for a small number of GBs in a few binary systems. Systematic investigations covering a wide range of temperatures all the way to the melting point are especially demanding. For this reason, only two GBs have been studied in the present work. As such, we selected two boundaries belonging to very different classes: a low-angle GB, which essentially represents a dislocation network, and a high-angle GB with a structurally homogeneous core. Although each boundary is characterized by specific set of crystallographic parameters, many of the conclusions of this work are generic and should be valid for all low-angle and all high-angle GBs, respectively. In particular, the fact that diffusion in the low-angle GB is slower and is characterized by a larger activation energy in comparison with the high-angle GB, is consistent with the existing body of experimental



data for many other alloy systems [39]. The retardation of Al diffusion by the presence of Mg atoms was found in both low-angle and high-angle GBs, as well as in the bulk liquid phase, which strongly suggests that this is a generic effect. It should also be noted that at most temperatures studied in this work, the high-angle GB was found to be structurally disordered. In fact, at high enough temperatures it becomes a liquid-like layer. Under such conditions, the specific bicrystallography of this boundary is unimportant and it can be considered a “generic” high-angle GB.

There are several findings in this paper whose explanation requires further research. One of them is the observation of the strongly elongated Mg clusters (atomic chains) in the high-angle GB. We hypothesize that such clusters, as well as other possible chemical heterogeneities in segregated Al GBs, can serve as precursors of Al-Mg intermetallic compounds during their nucleation in oversaturated alloys. The clustering trend also suggests that the GB solution has a miscibility gap. While this line of inquiry was not pursued in this work, it seems quite possible that Al-Mg GBs can exhibit 2D phases and phase transformations among them [14, 44]. Furthermore, it is likely that the Mg clusters act as traps for diffusion of Mg atoms, vacancies and interstitials. This would explain the relatively slow GB diffusion rate of Mg. However, further work is required to better understand the underlying atomic mechanisms.

Although the GB diffusivities reported here cannot be compared with experiments, the Mg GB segregation in Al has been studied by several experimental techniques, including atom probe tomography (APT). The experiments show that Mg strongly segregates to Al GBs in most cases [3–10]. However, deviation from this trend were also reported in the literature. For example, recent APT studies of Mg distribution after severe plastic deformation [45, 46] revealed Mg-depleted zones near GBs. These zones are explained [45] by inhomogeneous nature of the deformation process, namely, by the interaction of Mg atoms with moving dislocations in micro-deformation bands in the deformed microstructure. This highly non-equilibrium effect does not contradict the observation of equilibrium Mg segregation in this work as well as in previous reports.

On the simulation side, Mg GB segregation in nanocrystalline Al-Mg was recently studied by the lattice Monte Carlo (LMC) method [3]. This method is different from the potential-based off-lattice Monte Carlo simulations reported in this paper. In LMC simulations, the lattice remains rigid and the interaction parameters are fitted to experimental information within the regular solution approximation. GBs are defined as regions with modified values of the interaction parameters. Despite these differences, the LMC results are consistent with our work. For example, the segregation isotherm at 200°C and the alloy composition of about 5 at.%Mg (Figure 7a in [3]) predicts GB concentration of about 30 at.%Mg. Our simulations give the concentration of about 22 at.%Mg at 350 K (Fig. 3a). Furthermore, the interaction of Mg atoms with GBs was recently studied by first-principles calculations [38] using the  $\Sigma 5$  (201)[001] symmetrical tilt boundary as a model. The calculations confirm

a negative segregation energy of Mg driving GB segregation. At the temperature of 550 K, the peak Mg concentration in this boundary was found to be about 32 at.%Mg. Thus, calculations by different methods for different high-angle GBs in Al predict the segregation levels of Mg consistent with the present work. This agreement is reassuring and suggests that the results reported here reflect the generic nature of the Mg interaction with Al GBs.

## V. CONCLUSIONS

We have studied GB segregation and GB diffusion in the Al-Mg system by atomistic computer simulations combining MD and MC methods. A typical Al-5.5at.%Mg alloy and two representative (high-angle and low-angle) GBs were chosen as models. The conclusions can be summarized as follows:

- In agreement with previous reports, Mg strongly segregates to high-angle GBs and, to a lesser extent, to low-angle GBs composed of dislocations. At low temperatures, such as 350 K, the local chemical composition in GBs can exceed 20 at.%Mg.
- The amount of GB segregation increases with decreasing temperature. The effective free energy of GB segregation is estimated to be about  $-0.28$  eV/atom for the high-angle GB studied here and much smaller ( $\sim -0.01$  eV/atom) for the low-angle GB.
- Distribution of the segregated Mg atoms over a GB is highly non-uniform. In the high-angle tilt GB, the Mg atoms tend to form clusters containing 10 to 30 atoms, especially at low temperatures. Such clusters are elongated parallel to the tilt axis and are similar to linear atomic chains.
- At high temperatures approaching the solidus line, the high-angle GB studied here exhibits a premelting behavior by developing a highly disordered, liquid-like structure. By contrast, the low-angle GB does not premelt and can be overheated past the solidus line. While the individual dislocations do become disordered, the dislocation network itself remains intact, demonstrating an extraordinary thermal stability.
- Mg segregation strongly affects the rate of GB diffusion in Al-Mg alloys. Mg GB diffusion is slower than Al GB self-diffusion in pure Al. Furthermore, Mg segregation slows down the GB diffusion of Al itself. This diffusion retardation could be responsible for the microstructure stability in Al-Mg alloys.
- The diffusion retardation effect caused by the Mg segregation is primarily due to the significant (about a factor of two) increase in the activation energy of GB diffusion (Table II).
- Mg segregation reduces the anisotropy of GB diffusion.

- Mg diffusion in high-angle GBs is several orders of magnitude faster than diffusion in low-angle GBs at the same temperature.

In the absence of experimental data, the GB diffusion coefficients obtained in this work can provide useful reference information for further investigations of Al-Mg alloys. GB diffusion coefficients appear as input material parameters in many models describing processes such as precipitation aging, solute drag, and micro-creep to name a few.

**Acknowledgement:** R. K. K. and Y. M. were supported by the National Science Foundation, Division of Materials Research, under Award No.1708314.

- 
- [1] I. Polmear, D. StJohn, J. F. Nie and M. Qian, *Light alloys - Metallurgy of the Light Metals* (Butterworth-Heinemann, Oxford, UK, 2017), 5th edition.
- [2] S. Lathabai and P. G. Lloyd, The effect of scandium on the microstructure, mechanical properties and weldability of a cast Al-Mg alloy, *Acta Mater.* **50**, 4275 – 4292 (2002).
- [3] S. P. Pun, W. Wang, A. Khalajhedayati, J. D. Schuler, J. R. Trelewicz and T. J. Rupert, Nanocrystalline Al-Mg with extreme strength due to grain boundary doping, *Mater. Sci. Eng. A* **696**, 400–406 (2017).
- [4] A. Devaraj, W. Wang, R. Verumi, L. Kovarik, X. Jiang, M. Bowden, J. R. Trelewicz, S. Mathaudhu and A. Rohatgi, Grain boundary segregation and intermetallic precipitation in coarsening resistant nanocrystalline aluminum alloys, *Acta Mater.* **165**, 698–708 (2019).
- [5] J. Guillot, N. Valle, E. Maitre, S. Verdier and H. N. Migeon, Investigation on the magnesium segregation in low-magnesium aluminium alloys, *Surface and Interface Analysis* **42**, 735–738 (2010).
- [6] X. Y. Liu and J. B. Adams, Grain-boundary segregation in Al-10%Mg alloys at hot working temperatures, *Acta Mater.* **46**, 3467–3476 (1998).
- [7] X. Liu, X. Wang, J. Wang and H. Zhang, First-principles investigation of Mg segregation at  $\Sigma = 11(113)$  grain boundaries in Al, *J. Phys.: Condens. Matter* **17**, 4301–4308 (2005).
- [8] B. H. Lee, S. H. Kim, J. H. park, H. W. Kim and J. C. Lee, Role of Mg in simultaneously improving the strength and ductility of Al-Mg alloys, *Mater. Sci. Eng. A* **657**, 115–122 (2016).
- [9] M. J. Rahman, H. S. Zurob and J. J. Hoyt, Molecular dynamics study of solute pinning effects on grain boundary migration in the aluminum magnesium alloy system, *Metall. Mater. Trans. A* **47**, 1889–1897 (2016).
- [10] A. Kazemi and S. Yang, Atomistic study of the effect of magnesium dopants on the strength of nanocrystalline aluminum, *JOM* **71**, 1209–1214 (2019).
- [11] J. W. Cahn, The impurity-drag effect in grain boundary motion, *Acta Metall.* **10**, 789–798 (1962).

- [12] K. Lücke and H. P. Stüwe, On the theory of grain boundary motion, in *Recovery and Recrystallization of Metals*, edited by L. Himmel, pages 171–210 (Interscience Publishers, New York, 1963).
- [13] K. Lücke and H. P. Stüwe, On the theory of impurity controlled grain boundary motion, *Acta Metall.* **19**, 1087–1099 (1971).
- [14] Y. Mishin, Solute drag and dynamic phase transformations in moving grain boundaries, *Acta Mater.* **179**, 383–395 (2019).
- [15] R. Koju and Y. Mishin, Direct atomistic modeling of solute drag by moving grain boundaries, *Acta Mater.* **198**, 111–120 (2020).
- [16] N. Birbilis and R. G. Buchheit, Electrochemical characteristics of intermetallic phases in aluminum alloys: An experimental survey and discussion, *Journal of The Electrochemical Society* **152**, B140–B151 (2005).
- [17] J. Yan, N. Heckman, L. Velasco and A. M. Hodge, Improve sensitization and corrosion resistance of an Al-Mg alloy by optimization of grain boundaries, *Scientific Reports* **6**, 26870 EP (2016).
- [18] J. L. Searles, P. I. Gouma and R. G. Buchheit, Stress corrosion cracking of sensitized AA5083 (Al-4.5Mg-1.0Mn), *Metall. Mater. Trans. A* **32**, 2859–2867 (2001).
- [19] S. K. Das, N. Brodusch, R. Gauvin and I. H. Jung, Grain boundary diffusion of Al in Mg, *Scripta Mater.* **80**, 41–44 (2014).
- [20] W. Zhong, M. S. Hooshmand, M. Ghazisaeidi, W. Windl and J. C. Zhao, An integrated experimental and computational study of diffusion and atomic mobility of the aluminum-magnesium system, *Acta Mater.* **189**, 214–231 (2020).
- [21] A. Gangulee and F. M. d’Heurle, Mass transport during electromigration in aluminum-magnesium thin films, *Thin Solid Films* **25**, 317–325 (1975).
- [22] I. Kaur, W. Gust and L. Kozma, *Handbook of Grain and Interphase Boundary Diffusion Data* (Ziegler, Stuttgart, 1989).
- [23] M. I. Mendeleev, M. Asta, M. J. Rahman and J. J. Hoyt, Development of interatomic potentials appropriate for simulation of solid–liquid interface properties in Al–Mg alloys, *Philos. Mag.* **89**, 3269–3285 (2009).
- [24] M. I. Mendeleev, M. J. Kramer, C. A. Becker and M. Asta, Analysis of semi-empirical interatomic potentials appropriate for simulations of crystalline and liquid Al and Cu, *Philos. Mag.* **68**, 1723–1750 (2008).
- [25] D. Y. Sun, M. I. Mendeleev, C. A. Becker, K. Kudin, T. Haxhimali, M. Asta, J. J. Hoyt, A. Karma and D. J. Srolovitz, Crystal-melt interfacial free energies in hcp metals: A molecular dynamics study of Mg, *Phys. Rev. B* **73**, 024116 (2006).
- [26] S. Plimpton, Fast parallel algorithms for short-range molecular-dynamics, *J. Comput. Phys.* **117**, 1–19 (1995).
- [27] A. Stukowski, Visualization and analysis of atomistic simulation data with OVITO – the

- open visualization tool, *Model. Simul. Mater. Sci. Eng* **18**, 015012 (2010).
- [28] Y. Mishin and D. Farkas, Atomistic simulation of [001] symmetrical tilt grain boundaries in NiAl, *Philos. Mag. A* **78**, 29–56 (1998).
- [29] A. Suzuki and Y. Mishin, Atomistic modeling of point defects and diffusion in copper grain boundaries, *Interface Science* **11**, 131–148 (2003).
- [30] A. Suzuki and Y. Mishin, Interaction of point defects with grain boundaries in fcc metals, *Interface Science* **11**, 425–437 (2003).
- [31] B. Sadigh, P. Erhart, A. Stukowski, A. Caro, E. Martinez and L. Zepeda-Ruiz, Scalable parallel Monte Carlo algorithm for atomistic simulations of precipitation in alloys, *Phys. Rev. B* **85**, 184203 (2012).
- [32] A. Suzuki and Y. Mishin, Atomic mechanisms of grain boundary diffusion: Low versus high temperatures, *J. Mater. Sci.* **40**, 3155–3161 (2005).
- [33] J. W. Cahn, Y. Mishin and A. Suzuki, Coupling grain boundary motion to shear deformation, *Acta Mater.* **54**, 4953–4975 (2006).
- [34] R. K. Koju and Y. Mishin, Relationship between grain boundary segregation and grain boundary diffusion in Cu-Ag alloys, *Phys. Rev. Materials* **4**, 073403 (2020).
- [35] H. Sun and C. V. Singh, Temperature dependence of grain boundary excess free volume, *Scripta Mater.* **178**, 71–76 (2020).
- [36] J. P. Hirth and J. Lothe, *Theory of Dislocations* (Wiley, New York, 1982), 2nd edition.
- [37] D. McLean, *Grain Boundaries in Metals* (Clarendon Press, Oxford, 1957).
- [38] M. V. Petrik, A. R. Kuznetsov, N. A. Enikeev, Y. N. Gornostyrev and R. Z. Valiev, Peculiarities of interactions of alloying elements with grain boundaries and the formation of segregations in Al–Mg and Al–Zn alloys, *Physics of Metals and Metallography* **119**, 607–612 (2018).
- [39] I. Kaur, Y. Mishin and W. Gust, *Fundamentals of Grain and Interphase Boundary Diffusion* (Wiley, Chichester, West Sussex, 1995).
- [40] Y. Mishin, C. Herzig, J. Bernardini and W. Gust, Grain boundary diffusion: fundamentals to recent developments, *Int. Mater. Reviews* **42**, 155 (1997).
- [41] Y. Mishin and C. Herzig, Grain boundary diffusion: recent progress and future research, *Mater. Sci. Eng. A* **260**, 55–71 (1999).
- [42] T. Frolov, S. V. Divinski, M. Asta and Y. Mishin, Effect of interface phase transformations on diffusion and segregation in high-angle grain boundaries, *Phys. Rev. Lett.* **110**, 255502 (2013).
- [43] S. V. Divinski, H. Edelhoff and S. Prokofjev, Diffusion and segregation of silver in copper  $\Sigma 5$  (310) grain boundary, *Phys. Rev. B* **85**, 144104 (2012).
- [44] T. Frolov and Y. Mishin, Phases, phase equilibria, and phase rules in low-dimensional systems, *J. Chem. Phys.* **143**, 044706 (2015).
- [45] J. Xue, S. Jin, X. An, X. Liao, J. Li and G. Sha, Understanding formation of Mg-depletion

- zones in Al-Mg alloys under high pressure torsion, *Journal of Materials Science & Technology* **35**, 858–864 (2019).
- [46] X. Sauvage, A. Duchaussoy and G. Zaher, Strain induced segregations in severely deformed materials, *Materials Transactions* **60**, 1151–1158 (2019).

Grain boundary	$F_s$ (eV)	$\alpha$	$R^2$
$\Sigma 17(530)[001]$ tilt	$-0.281 \pm 0.004$	$0.166 \pm 0.001$	98.39%
$\Sigma 3601(001)$ twist	$-0.014 \pm 0.001$	$0.891 \pm 0.021$	93.88%

Table I: Segregation free energy and the fraction of available segregation sites extracted from the simulation results. The last column reports the  $R^2$  coefficient of determination characterizing the quality of fit by the Langmuir-McLean model in Eq.(2).

	Direction	Al in pure Al	Al in alloy	Mg in alloy
$\Sigma 17(530)[001]$ GB				
$E$ (eV)	$\parallel$ tilt axis	$0.73 \pm 0.02$	$1.22 \pm 0.05$	$1.52 \pm 0.08$
	$\perp$ tilt axis	$0.83 \pm 0.01$	$1.27 \pm 0.03$	$1.54 \pm 0.06$
$D_0$ (m <sup>2</sup> /s)	$\parallel$ tilt axis	$(3.33_{-0.90}^{+1.23}) \times 10^{-6}$	$(2.60_{-1.48}^{+3.45}) \times 10^{-3}$	$(8.48_{-6.06}^{+21.26}) \times 10^{-2}$
	$\perp$ tilt axis	$(1.57_{-0.28}^{+0.34}) \times 10^{-5}$	$(5.38_{-2.16}^{+3.60}) \times 10^{-3}$	$(1.12_{-0.72}^{+1.99}) \times 10^{-1}$
$\Sigma 3601(001)$ GB				
$E$ (eV)	$\perp$ twist axis	$0.66 \pm 0.04$	$1.16 \pm 0.09$	$1.18 \pm 0.06$
$D_0$ (m <sup>2</sup> /s)	$\perp$ twist axis	$(1.33_{-0.55}^{+0.93}) \times 10^{-8}$	$(1.27_{-0.94}^{+3.56}) \times 10^{-5}$	$(1.47_{-0.86}^{+2.08}) \times 10^{-5}$

Table II: The activation energy  $E$  and pre-exponential factor  $D_0$  for GB diffusion in pure Al and in the Al-Mg alloy.

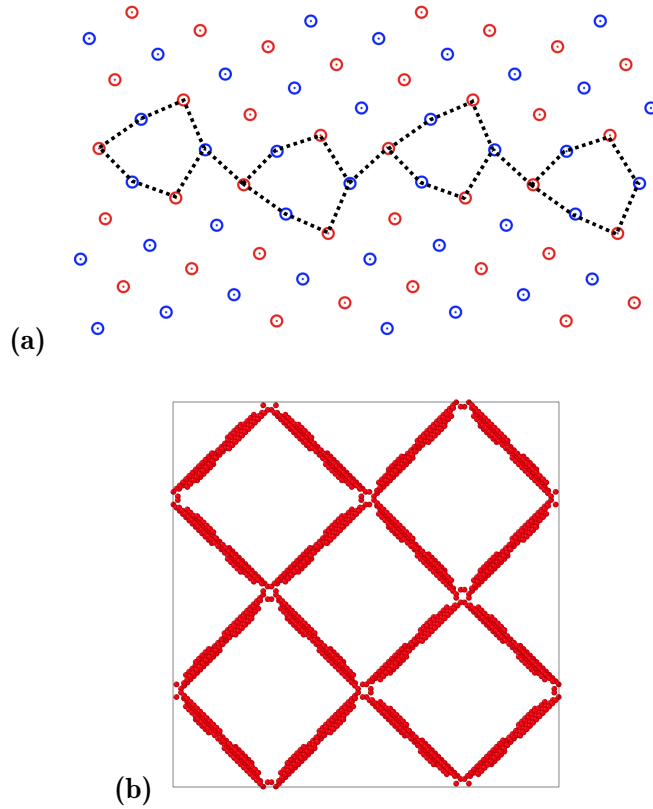


Figure 1: Structures of the GBs studied in this work. (a) Symmetrical tilt  $\Sigma 17(530)[001]$  GB composed of kite-shape structural units. The structure is projected along the  $[001]$  tilt axis normal to the page. The GB plane is horizontal. The open and filled circles represent atoms located in alternating  $(002)$  planes parallel to the page. The structural units are outlined by dotted lines. (b) Top view of the  $\Sigma 3601(001)$  twist GB composed of  $\frac{1}{2} \langle 110 \rangle$  edge dislocations. The  $\{001\}$  GB plane is parallel to the page. The dislocations are visualized by the bond-order analysis using OVITO [27]. The perfect-lattice atoms are removed for clarity.



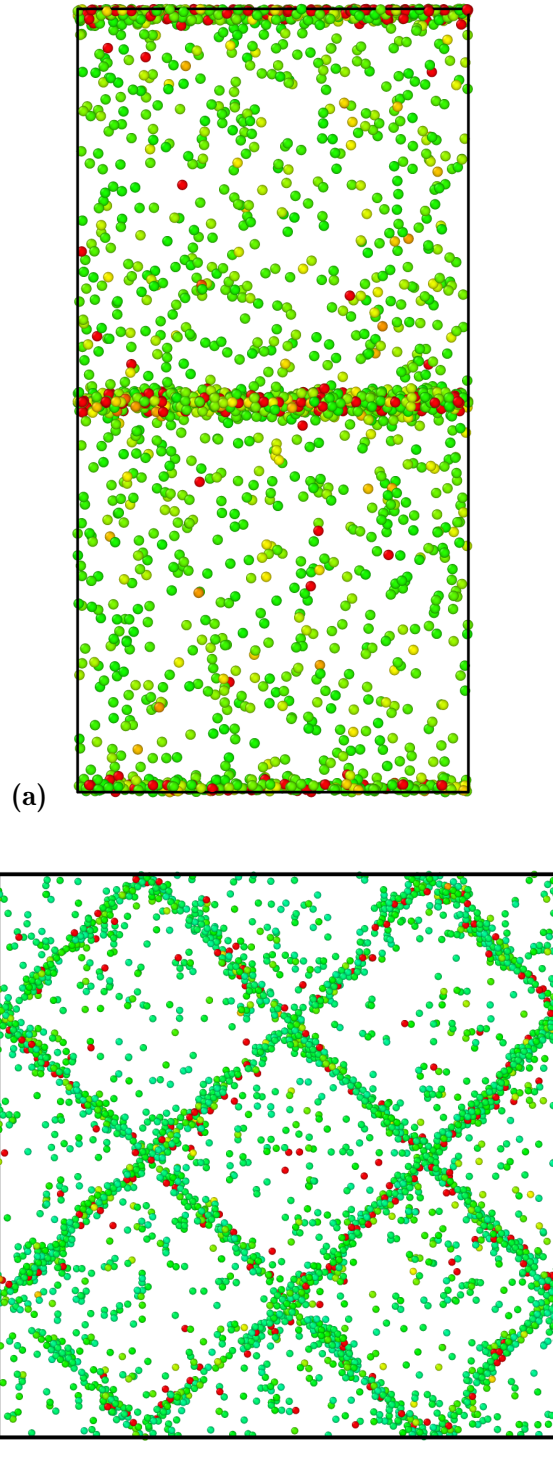


Figure 2: GB structure at the temperature of 700 K. (a) Symmetrical tilt  $\Sigma 17(530)[001]$  GB. (b)  $\Sigma 3601(001)$  twist GB. The grain orientations are the same as in Figure 1. The green color represents the most distorted Al atoms with the centrosymmetry parameter above a threshold value. The red color represents Mg atoms. The images have been generated using OVITO [27].

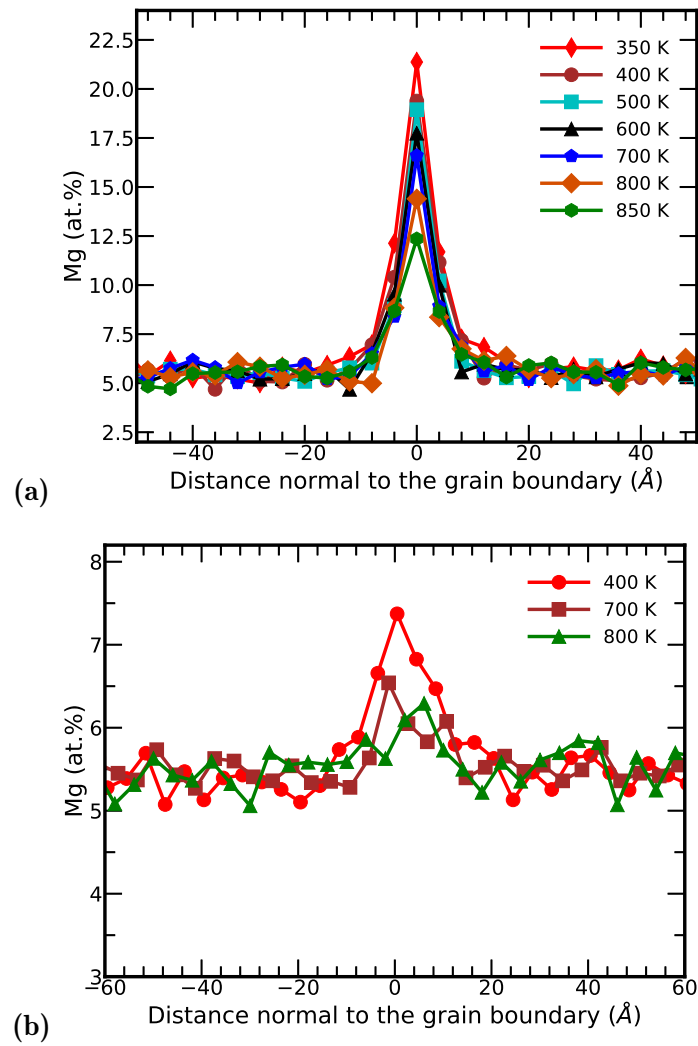
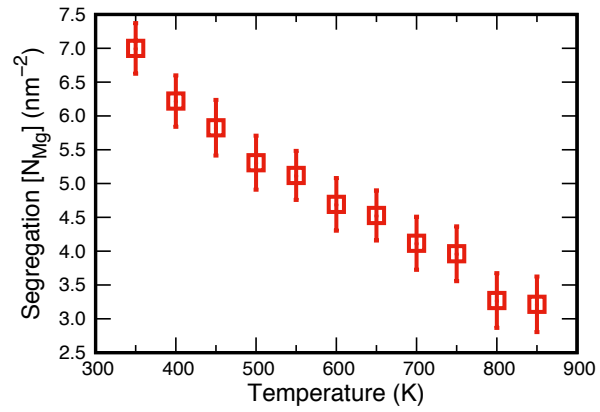
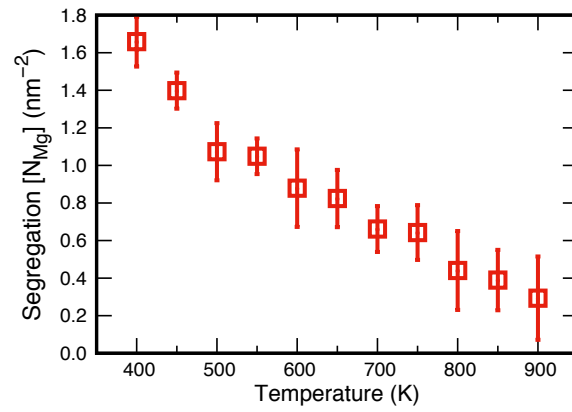


Figure 3: Mg segregation profiles in (a)  $\Sigma 17(530)[001]$  tilt GB and (b)  $\Sigma 3601(001)$  twist GB at several temperatures. The alloy composition is Al-5.5at.%Mg.



(a)



(b)

Figure 4: Mg segregation in the Al-5.5at.%Mg alloy as a function of temperature for the (a)  $\Sigma 17(530)[001]$  tilt GB and (b)  $\Sigma 3601(001)$  GB. The error bars represent one standard deviation from averaging over multiple snapshots.

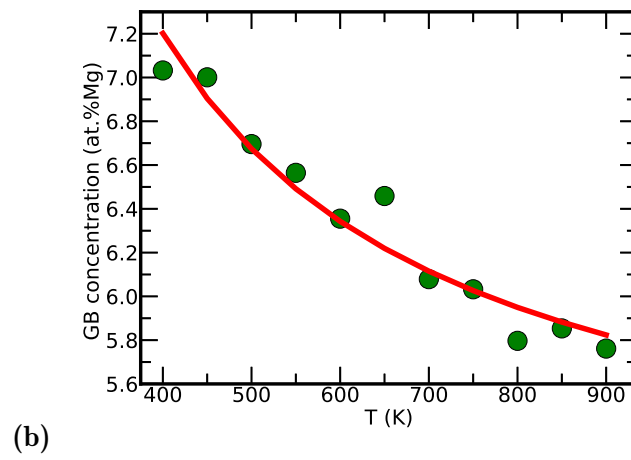
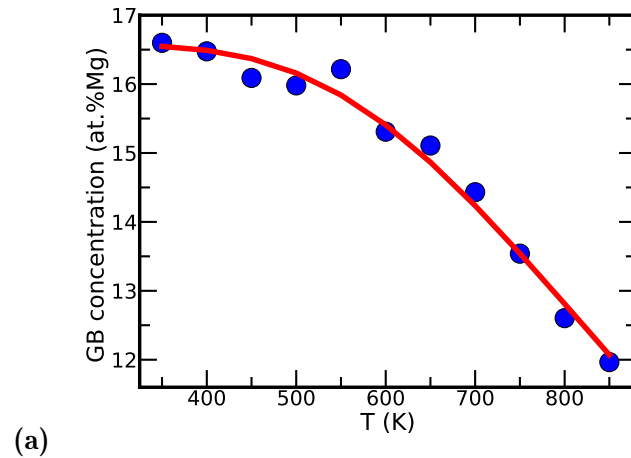


Figure 5: Mg atomic fraction in the (a)  $\Sigma 17(530)[001]$  tilt GB and (b)  $\Sigma 3601(001)$  GB as a function of temperature. The points represent simulation results while the curves were obtained by fitting the Langmuir-McLean model in Eq.(2).

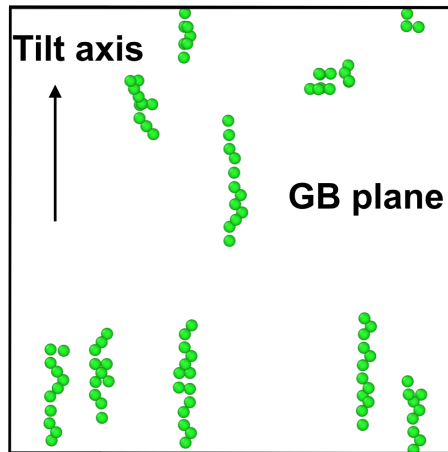
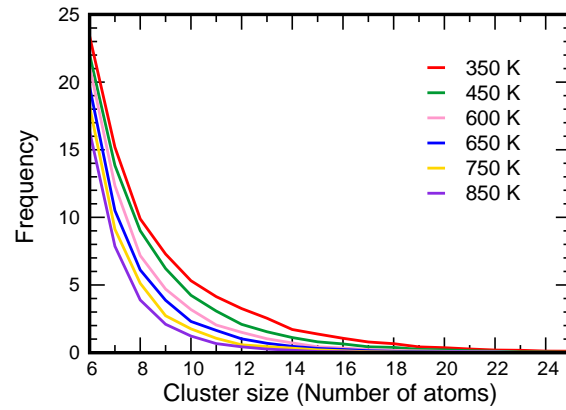
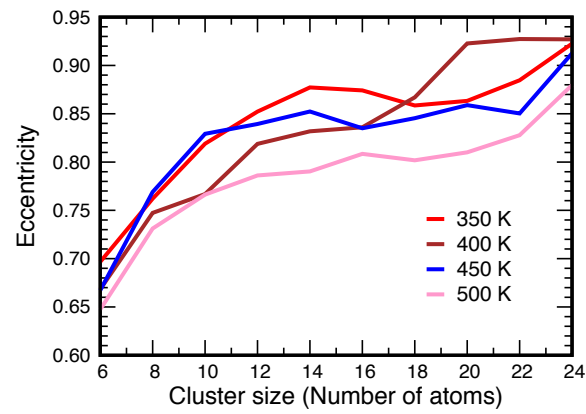


Figure 6: Mg clusters in the  $\Sigma 17(530)[001]$  tilt GB at 400 K. The GB plane is parallel to the page. Only clusters containing 10 or more atoms are shown for clarity.



(a)



(b)

Figure 7: Size and shape of Mg clusters in the  $\Sigma 17(530)[001]$  tilt GB at selected temperatures. (a) Size distribution. The vertical axis gives the number of clusters of a given size in the simulation block averaged over multiple snapshots. (b) Eccentricity of the clusters, given by Eq.(3), plotted as a function of the cluster size.

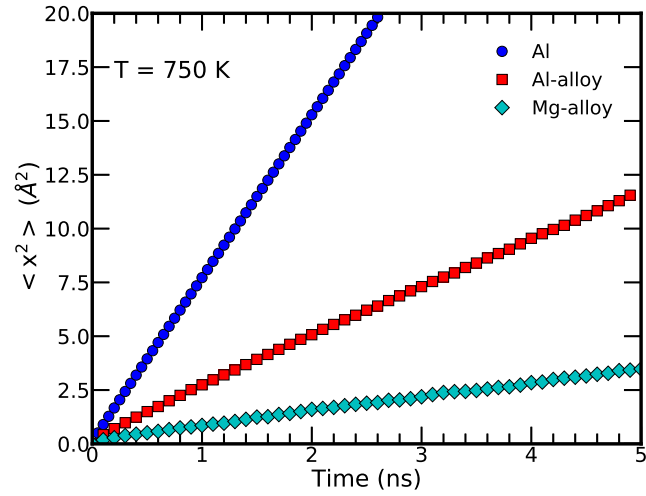


Figure 8: Mean-square atomic displacement normal to the tilt axis versus time in the  $\Sigma 17(530)[001]$  GB at the temperature of 750 K. The lines represent GB self-diffusion in pure Al and GB diffusion of Al and Mg in the Al-5.5at.%Mg alloy.

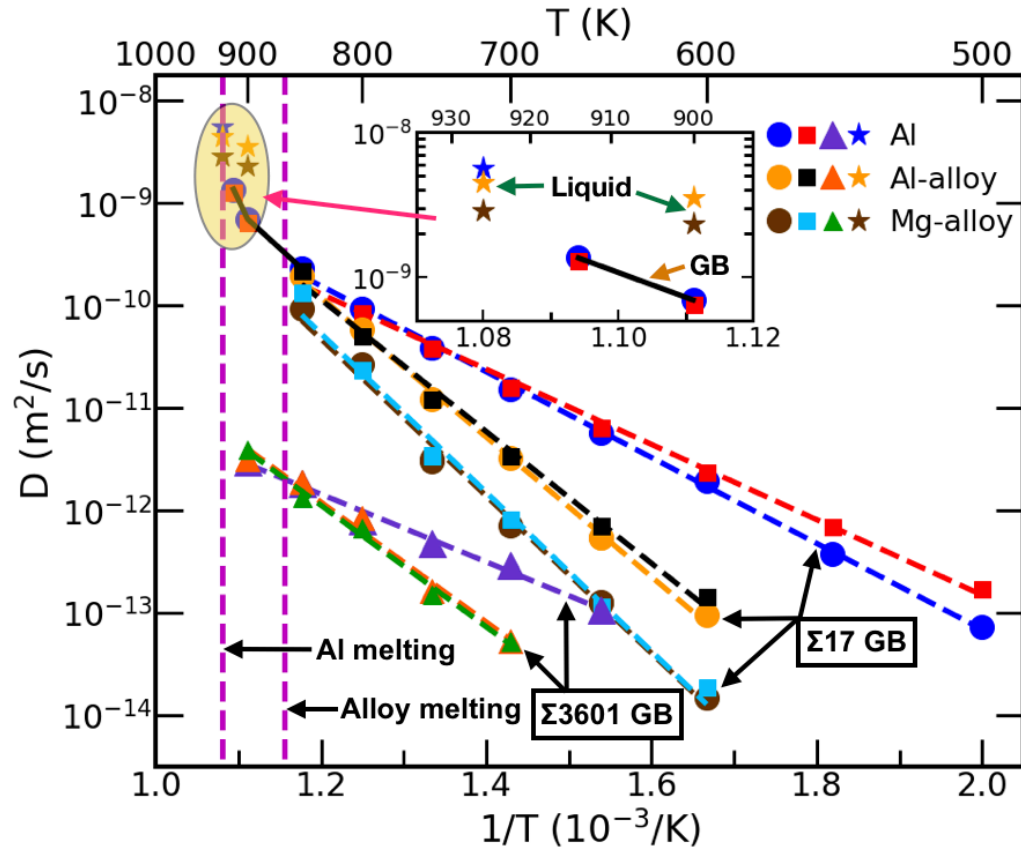


Figure 9: Arrhenius diagram of GB diffusion coefficients (points) and their linear fits (dashed lines). The square and circle symbols represent diffusion parallel and normal to the tilt axis, respectively, in the high-angle GB. The triangular symbols represent diffusion in the low-angle GB. The inset is a zoom into the high-temperature region showing diffusion in liquid Al and the liquid alloy (star symbols).